Am J Transl Res 2023;15(2):878-895
www.ajtr.org /ISSN:1943-8141/AJTR0144430

Original Article

A novel NSUN5/ENO3 pathway promotes the Warburg effect and cell growth in clear cell renal cell carcinoma by 5-methylcytosine-stabilized ENO3 mRNA

Juan Wang[1], Hong-Juan Ju[1], Fan Zhang[1], Hui Tian[1], Wen-Gang Wang[1], Yu-Lin Ma[1], Wen-Sheng Xu[1], Yue-Heng Wang[2]

[1]*Department of Abdominal Ultrasound, The Second Hospital of Hebei Medical University, 215 Heping West Road, Shijiazhuang 050000, Hebei, China;* [2]*Department of Cardiac Ultrasound, The Second Hospital of Hebei Medical University, Shijiazhuang 050000, Hebei, China*

Received May 28, 2022; Accepted January 11, 2023; Epub February 15, 2023; Published February 28, 2023

Abstract: Objectives: Clear cell renal cell carcinoma (ccRCC) cells often reprogram their metabolisms. Enolase 3 (ENO3) is closely related to the Warburg effect observed in cells during tumor progression. However, the expression and function of ENO3 in ccRCC cells remain unclear. Therefore, this study investigated the expression and functional significance of ENO3 in the Warburg effect observed in ccRCC cells. Methods: In this study, B-mode and microflow imaging ultrasound examinations were performed to evaluate patients with ccRCC. The extracellular acidification rate test and glucose uptake and lactate production assays were used to examine the Warburg effect in ccRCC cells. Western blotting, quantitative reverse transcription polymerase chain reaction, and immunochemistry were used to detect the expression of ENO3 and NOP2/Sun RNA methyltransferase 5 (NSUN5). Results: ENO3 upregulation in ccRCC tumor tissues was accompanied by an increase in tumor size. Importantly, ENO3 participated in the Warburg effect observed in ccRCC cells, and high levels of ENO3 indicated a poor prognosis for patients. Loss of ENO3 reduced glucose uptake, lactate production, and extracellular acidification rate as well as inhibited ccRCC cell proliferation. Furthermore, NSUN5 was involved in the ENO3-regulated Warburg effect and ccRCC cell progression. Mechanically, NSUN5 was upregulated in ccRCC tissues, and NSUN5 upregulation mediated 5-methylcytosine modification of messenger RNA (mRNA) in ccRCC cells to promote mRNA stability and ENO3 expression. Conclusions: Collectively, the destruction of the NSUN5/ENO3 axis prevents ccRCC growth *in vivo* and *in vitro,* and targeting this pathway may be an effective strategy against ccRCC progression.

Keywords: Enolase 3, NSUN5, Warburg effect, 5-methylcytosine, clear cell renal cell carcinoma

Introduction

Renal cell carcinoma (RCC) is the most deadly urinary tract tumor [1]. Approximately 70,000 new renal cancer cases are reported annually in China, with approximately 23,000 deaths [2]. The incidence and mortality of RCC have gradually increased over the past few decades. Clear cell RCC (ccRCC) is the most common histological type of RCC, accounting for approximately 80% of all RCC cases [3]. Although surgery, inhibitor drugs, and immunotherapy have prolonged the lives of patients with RCC to a certain extent, its clinical effects observed in the past decade have been unsatisfactory [4-6]. One of the reasons is that RCC pathogenesis remains poorly understood. However, increasing evidence suggests that RCC is a metabolic disease [7, 8]. It is usually accompanied by the reprogramming of glucose and fatty acid metabolism [9]. For example, even under normal oxygen concentrations, tumor cells undergo anaerobic glycolysis to utilize glucose and increase lactic acid production, also known as the Warburg effect [10]. Recent studies have shown that the Warburg effect plays an important role in tumor development and progression [11, 12]. Reports implied that the Warburg effect is stronger in the volume of large tumors than small tumors [13, 14]. Many studies have reported heterogeneous expression of energy metabolism-associated genes in RCC cells,

indicating that the Warburg effect may be involved in RCC development [15, 16]. However, the role of the Warburg effect in RCC development and the underlying mechanism remain largely unknown.

Enolase (ENO) is a metalloenzyme, also known as 2-phospho-D-glycerate hydrolase [17, 18]. In eukaryotes, this family of proteins includes three different subtypes: ENO1 or α-ENO, ENO2 or γ-ENO, and ENO3 or β-ENO. All three enzymes can catalyze glycolysis progression and have unique functions. Enolase-1 (ENO1) plays a role in fibrinolysis in blood vessels and around cells; enolase-2 (ENO2) promotes the nutrition and protection of the central nervous system; and enolase-3 (ENO3) regulates the development and regeneration of striated muscle [19]. Studies have shown that they participate in the glycolysis pathway and catalyze the dehydration of 2-phospho-D-glyceric acid to phosphoenolpyruvate. Many studies have revealed that ENO, especially ENO1 and ENO2, plays an important role in various tumors [20-22]. Like the other two types, ENO3 also plays an important role in tumors, although studies on this are rare. A previous study showed that ENO3 knockdown inhibits the proliferation of lung cancer cells with mutated serine/threonine-protein kinase 11 (STK11) and that it has selective anticancer effects [23]. In colorectal cancer, low ENO2 and ENO3 expression is significantly associated with longer overall survival [24], indicating that ENO3 is closely related to tumor development. Studies have also shown that ENO3 is related to the Warburg effect [25, 26]. However, the expression level and function of ENO3 in ccRCC cells remain unexplained. Therefore, in our study, we investigated ENO3 expression and its functional significance in the Warburg effect observed in ccRCC cells.

NSUN5, a member of the Nop2/SUN domain family, is a conserved RNA methyltransferase [27]. NSUN family consists of 6 members, such as Nsun2 (Misu), Nsun3, Nsun4, Nsun5 (Wbscr20, Wbscr20a), Nsun6 (NOPD1) and Nsun7 [28]. NSUN5 is associated with various diseases, a study reported that NSUN5 is closely related to the occurrence of tetralogy of Fallot [29]. In addition, research showed that NSUN5 regulated cell proliferation by regulating cell cycle in colorectal cancer [28]. In recent years, some studies have demonstrated that NSUN5 plays an important role in tumors. However, the role of NSUN5 in ccRCC is largely unclear. In this study, we found that the upregulation of ENO3 promoted cell growth and enhanced the Warburg effect in ccRCC. NSUN5-mediated m5C modification promoted ENO3 expression by stabilizing mRNA.

Materials and methods

Subjects

Our study included forty-nine East Asian patients with ccRCC living in China [35 males and 14 females; 31-74 years old, mean age: 57.7±8.5 years; mean BMI: 30.1±5.0 kg/m^2; two were single, and the rest were married; all had medicaid and insurance; there were four males and one female who had type 2 diabetes; twenty-three patients (16 males and seven females) were obese]. All the patients underwent B-mode and microflow imaging (MFI) ultrasound examinations (Department of Ultrasound) and surgical treatment (Department of Urology) at the Second Hospital of Hebei Medical University from November 2018 to October 2021. All ccRCC lesions were diagnosed via intraoperative and pathological findings. The study patients did not report having a history of chronic renal disease, and their renal function test results, such as urea nitrogen and creatinine, were normal. The kidney tissue in our study excluded tissue from patients with simultaneous bilateral renal tumors, patients with multiple tumors in one kidney, and patients with a family history of RCC or a history of hereditary RCC syndrome. Informed consent was obtained from the patients before the examination. The Human Ethics Committee of the Second Hospital of Hebei Medical University approved all the experimental protocols of this study (No. 2018-R131).

B-mode and MFI

We performed B-mode and MFI detection on patients using a C5-1 curve sensor with MFI imaging software and a Philips EPIQ7 (USA) [30]. The presence of renal tumors was investigated, and B-ultrasound technology was used to evaluate tumor size. The following ICD-10 classification codes were included: C64.1 (malignant neoplasm of the right kidney, except

the renal pelvis) and C64.2 (malignant neoplasm of the left kidney, except the renal pelvis). To accurately determine the location, borders, and echo patterns of renal tumors and to measure tumor size, MFI ultrasound was performed to detect the tumor's capillaries and low-velocity blood flow, and static and dynamic images were recorded. The scale and color gain of MFI were adjusted to obtain the strongest blood vessel signal, whereas the background color interference had the least. During image acquisition, minimal pressure was applied using the ultrasound probe.

Primary cell cultures

Fresh ccRCC tissue was immediately washed twice with ice-cold normal saline and immersed in cold Roswell Park Memorial Institute (RPMI) 1640 medium (Gibco), including 1% penicillin/streptomycin (Gibco) and 0.5% glutamine. As described previously [31], cell culture was performed within 60 min after surgery. Briefly, the surrounding adipose tissue, blood vessels, and necrotic tissue were removed, and the tumor tissue was cut using scissors. We washed the tumor cells twice with serum-free RPMI 1640 medium. Cells were resuspended in added 20% fetal bovine serum (FBS), 2-mmol/L L-glutamine, 100 units/mL penicillin, and 100-μg/mL streptomycin with RPMI 1640 medium (Gibco). Then they were incubated at 37°C, 5% CO_2, and 95% humidity. Cells were passaged to approximately 80% confluence. The third to the fifth generations of ccRCC cells were used for performing experiments.

Cell lines and transfection

We purchased human ccRCC cell lines (A498, SW839, Caki-1, and 786-0) and 293A cells from the American Type Culture Collection and stored them at the Molecular Biology Laboratory of the Second Hospital of Hebei Medical University. Also, we cultured all cells in Dulbecco's Modified Eagle Medium (Gibco) containing 10% FBS and 1% penicillin/streptomycin (Gibco). The incubator used to culture the cells was set to contain 95% air and 5% CO_2. Cells were transfected with Lipofectamine 2000 (Invitrogen) when they were around 70% grown. The overexpression/control plasmid was constructed and purchased from Biocaring Biotechology (Shijiazhuang, Hebei). Each 25 square centimeter cell flask was transfected with three micrograms of plasmid and 15 microliters of Lipo2000. siRNA was purchased from Gema Company, Ltd. (Shanghai, China) and the sequences were shown in Table S1. The dose of siRNA transfection was 100 pmol.

Glucose uptake and lactate production assays

Cellular glucose consumption and lactate production were measured as in previous studies [32]. 1×10^5 cells were seeded in 12-well plates and incubated in an incubator for 24 h. The medium was collected and analyzed using the Bioprofile Flex analyzer (BP-Flex). The glucose test kit, GAGO20-1KT (Sigma-Aldrich), was used for glucose consumption according to the manufacturer's recommendations. The lactic acid content was analyzed using a lactic acid detection kit (1200011002; Eton Biosciences).

Extracellular acidification rate (ECAR) test

Cells (1×10^4) were seeded into a Seahorse XF 24-well microplate and incubated for 24 h. An Agilent Seahorse XFe24 analyzer was used to detect ECAR according to the previously described method [32]. Before performing the measurements, cells were placed in a CO_2 incubator for one hour to exclude their influence on the pH value, and a baseline measurement was performed. According to the designed protocol, glucose, oligomycin (oxidative phosphorylation inhibitor), and 2-deoxy-D-glucose glycolysis inhibitor were sequentially injected into every well. All results were processed via Seahorse Biosciences Wave software.

RNA isolation and real-time quantitative polymerase chain reaction (RT-qPCR)

Total RNA from tumor tissues or cultured cells was separated and extracted using Total RNA Kit I (Omega Bio-Tek) according to the manufacturer's instructions. The concentration and quality of total RNA were measured using NanoDrop 2000 (Thermo). MonScript RTIII Super Mix with dsDNase (Monad, China) and oligo-dT primer was used to synthesize the first-strand cDNA. MonAmp ChemoHS qPCR Mix kit (Monad) and C1000 Touch Thermal Cycler System (Bio-Rad) were used to detect mRNA expression. The relative transcription expression level was normalized to that of glyceraldehyde 3-phosphate dehydrogenase, and the

$2^{-\Delta\Delta Ct}$ formula was used as previously described [33]. The corresponding primers are listed in Table S2.

Western blotting

Protein lysis buffers were used to extract proteins from cultured cells and frozen clinical tissue samples. Sodium dodecyl sulfate-polyacrylamide gel electrophoresis experiments were used to separate proteins from protein samples, and the proteins were transferred to polyvinylidene fluoride membranes (Millipore) via semi-dry transfer [34]. The membrane was blocked with 5% nonfat milk for two hours at 37°C, then washed with milk and blocked with primary antibody overnight at 4°C. The membrane was incubated with 5% skimmed milk for two hours and treated with primary antibodies overnight at 4°C. Primary antibodies against ENO3 (1:1000; ab126259), NSUN5 (1:500; ab121633), CDK6 (1:1000; ab124821), and β-actin (1:1000; ab8226) were used. The next day, the primary antibody was washed with TTBS wash, and then the membrane was incubated with a horseradish peroxidase-conjugated secondary antibody (1:8000; Rockland) for two hours at room temperature. The protein bands on the membrane were visualized using a chemiluminescence meter. Images were captured and processed using Series Capture Software (Azure Biosystems).

Xenograft animal

Male BALB/c nude mice (18-22 g; 4-6 weeks old) were purchased from Weitahe Experimental Animal Technology Co., Ltd. (China) and used to develop the xenotransplantation animal model. 786-0 cells (5×10^6) with stable knockdown of ENO3, NSUN5, or both were resuspended in a phosphate-buffered saline medium bottle and mixed with 50% Matrigel (BD), constituting a total volume of 200 uL. The mixed suspension was injected subcutaneously on the dorsal side. One week after the cells were injected subcutaneously into the mice, tumor growth was measured twice weekly, and the length and width of the tumors were recorded. The following formula was used to count the tumor volume: tumor volume = (length × width^2)/2. After 28 days, mice were euthanized via carbon dioxide asphyxiation [33-35]. The Human Ethics Committee of the Second Hospital of Hebei Medical University approved the animal model protocols used in this study (No. 2018-AE107).

Morphometry and histology

Hematoxylin-eosin staining was used to determine the morphological measurement and histology, as described previously [35, 36]. We fixed ccRCC and normal kidney tissue in formalin solution for 24 h, followed by routine dehydration and paraffin embedding. Sections (5-μm) were used for hematoxylin-eosin or immunochemistry staining (ENO3 antibody). Staining results were photographed using a Leica microscope (Leica DM6000B, Switzerland), followed by digital analysis with LAS version 4.4 (Leica).

Immunohistochemical staining

Immunohistochemical staining was performed as described previously [34]. Paraffin tissue sections were first deparaffinized with xylene, followed by gradient dehydration with ethanol. Next, the cells were treated with hydrogen peroxide and blocked using goat serum. The protein antibody was diluted according to a certain ratio, and the tissue sections were incubated with the primary antibody overnight at 4°C. The next day, they were placed at room temperature for 30 min, aspirated the surface antibody of the tissue, and incubated the tissue with the secondary antibody for 30 min at 37°C. Tissue sections were added dropwise to horseradish enzyme-labeled streptavidin working solution at 37°C for 20 min. Then, an appropriate amount of DAB stain developing solution was added dropwise at room temperature. After the sections were washed and stained with hematoxylin, they were gradually dehydrated, made transparent, and mounted.

Immunofluorescence staining

As previously described, xenograft tissue sections were routinely deparaffinized and dehydrated [35]. After antigen retrieval, tissue sections were sealed with goat serum and incubated overnight with ENO3 (1:50, ab126259) and CDK6 (1:50, ab241554). Then, the tissues were treated with fluorescein-labeled anti-rabbit IgG (KPL) and rhodamine-labeled anti-mouse IgG (KPL) [37]. Nuclei were stained with 4,6-diamidino-2-phenylindole (157574; MB Biomedical) was used for nuclear staining.

Images were captured using a confocal microscope (Leica) and processed using the LAS AF software.

3-(4,5-dimethylthiazol-2-yl)-5-(3-carboxymethoxyphenyl)-2-(4-sulfophenyl)-2H-tetrazolium (MTS) assay

The cell viability was checked using an MTS assay following the kit instruction manual (ab197010) [35]. We seeded 1000 786-0 and Caki-1 cells into 96-well plates and transfected the corresponding vectors according to the experimental needs. MTS reagent (20 μL) was added to each well, and the cells were incubated in a 37°C cell incubator for 0.5-4 h. Finally, a microplate reader was used to measure the absorbance of cells at 490 nm (Thermo Fisher).

m5C RNA immunoprecipitation (MeRIP) assay

MeRIP-qPCR was used according to the reported method (6). Total RNA was extracted from clinical tissue samples or cell lines. Total RNA was isolated and treated with DNase I to avoid DNA contamination. The RNA concentration was adjusted to 1 μg/μL using nuclease-free water. According to the GenSeq m5C MeRIP kit (Cloudseq) standard protocol, RNA was chemically fragmented to ~200 nt, and the fragmented RNA was immunoprecipitated with an anti-m5C antibody. Primers were designed for the m5C enrichment region of ENO3 (the two sites were 261 and 407), and the m5C enrichment amount was determined using qPCR. All data were analyzed using the $2^{-\Delta\Delta Ct}$ method.

Bioinformatics analysis

The relationship between *ENO3* and *NSUN5* expression and ccRCC patients' prognosis was analyzed using bioinformatics analysis. The expression of *ENO3* and *NSUN5* in ccRCC cells was analyzed online through http://ualcan.path.uab.edu/analysis.html and obtained through http://www.oncolnc.org/. Kaplan-Meier analysis was used to analyze the relationship between their expression and the patients' prognosis.

Statistical analysis

Data were expressed as mean ± standard error of the mean. An independent-samples t-test was used to analyze the differences between the two groups; and three or more groups make comparisons by the one-way ANOVA with Post Hoc Tests or Tukey's test. $P < 0.05$ was used to indicate statistical significance. GraphPad Prism version 7.0 was used for all statistical analyses.

Results

The Warburg effect enhances as the ccRCC tumor size increases

To investigate whether the Warburg effect is related to the ccRCC tumor size, patients with different tumor sizes were evaluated using B-mode ultrasound results. Reports suggest that the Warburg effect is stronger in large tumors [13, 14]. The study also showed that the Warburg effect is related to tumor size. To maintain the gap in tumor volume, we collected samples with volumes greater than 5 cm. This study used 5 cm as the threshold because 5 cm is the median diameter of these samples. As shown in **Figure 1A**, tumors were divided into two grades based on their volume-tumors with diameters < 5 cm and those with diameters > 5 cm. Hematoxylin-eosin staining was used to confirm normal (N) renal and tumor tissues of different sizes (**Figure 1B**). To explore whether the Warburg effect is related to tumor size, primary cells were isolated and cultured from the tumor tissues of patients with ccRCC, and the related Warburg effect experiment was performed. Compared to normal renal cells, the amount of glucose uptake by ccRCC cells increased with increasing tumor volume (**Figure 1C**). Consistently, similar results were found in the lactic acid production analysis and ECAR assays (**Figure 1D** and **1E**). Furthermore, the MTS assay results revealed that cell viability increased with increasing tumor volume (**Figure 1F**). These findings suggest that ccRCC cells derived from large tumors exhibit a stronger Warburg effect.

ENO3 expression increases in ccRCC tissues and leads to a poor prognosis

To identify the genes involved in the Warburg effect associated with ccRCC tumor size, candidate aerobic glycolysis-related genes were examined using RT-qPCR. As shown in **Figure 2A**, PKM, ENO3, PGAM1, PGAM2, and LDHA expression significantly increased in RCC tissues compared to normal tissues. However,

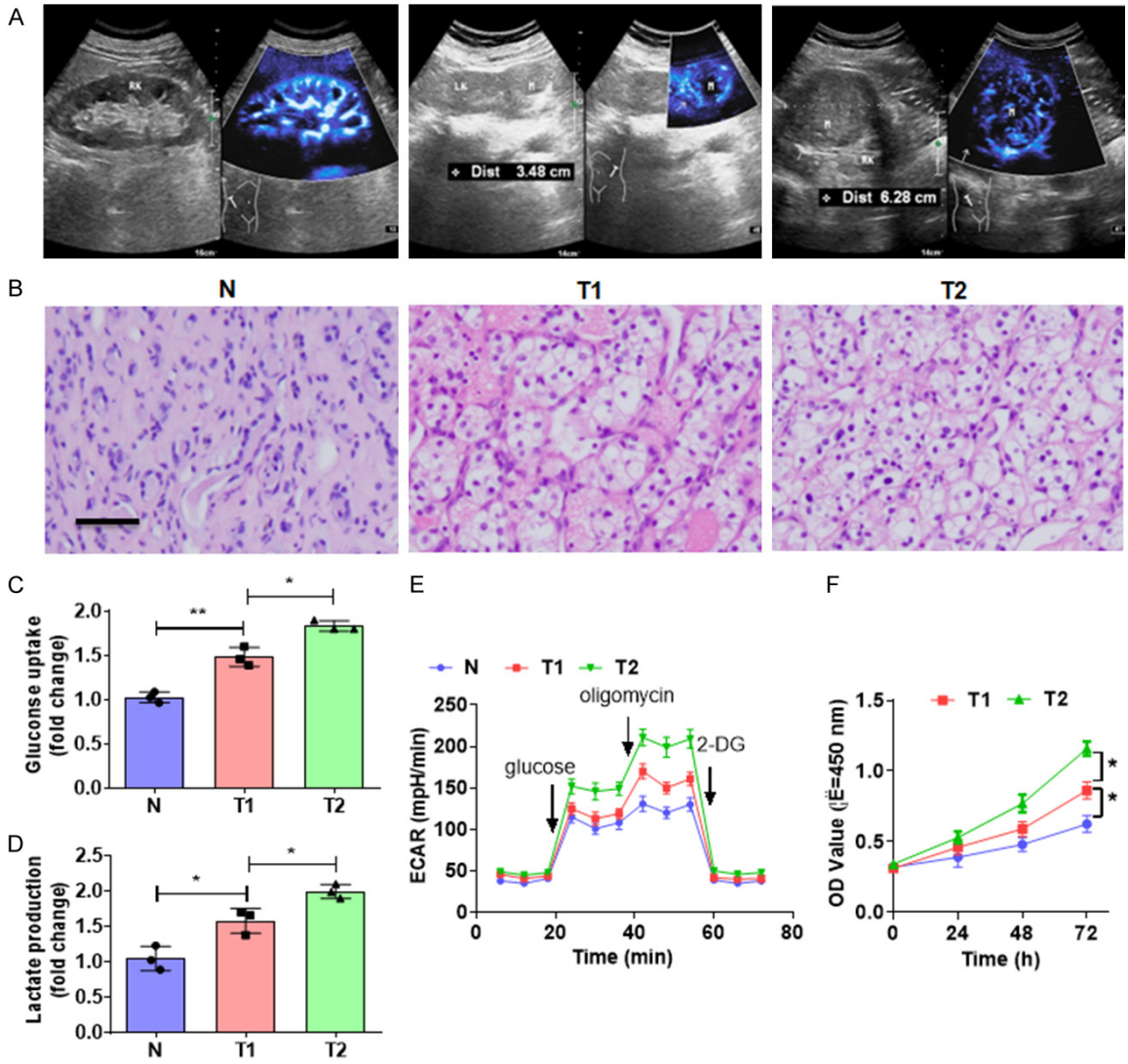

Figure 1. The Warburg effect of ccRCC (clear cell renal cell carcinoma) tumor cells enhances with the increase in tumor volume. A. B-mode and MFI (microflow imaging) ultrasound showed an isoechoic mass in the upper pole of the kidney (arrows). N, normal; T1, ccRCC (clear cell renal cell carcinoma) tumor diameter < 5 cm; T2, ccRCC (clear cell renal cell carcinoma) tumor diameter ≥ 5 cm. B. Hematoxylin-eosin staining confirmed different sizes of ccRCC (clear cell renal cell carcinoma) (T) and normal (N) kidney tissues. Scale bar, 50 μm. C. Primary ccRCC (clear cell renal cell carcinoma) cells isolated from the above clinical samples (N, T1, and T2), and glucose uptake analysis detected glucose consumption in these cells. D. Lactic acid production analysis revealed the amount of lactic acid produced in primary cells of kidney cancers of different sizes. E. ECAR (extracellular acidification rate) test was used to analyze the extracellular acidification efficiency of primary cells of renal cancer tissues of different sizes. F. The MTS (3-(4,5-dimethylthiazol-2-yl)-5-(3-carboxymethoxyphenyl)-2-(4-sulfophenyl)-2H-tetrazolium) assay was used to detect cell viability in primary cells of RCC (renal cell carcinoma) of different sizes. Data are expressed as mean ± standard error of the mean from three independent experiments. *P < 0.05, **P < 0.01 vs. corresponding controls.

only ENO3 expression increased as the tumor size increased. Subsequently, Western blotting and RT-qPCR results confirmed that ENO3 expression increased as the ccRCC size increased (**Figure 2B** and **2C**). In parallel, immunohistochemical staining revealed that the number of ENO3-positive cells increased as the size of the tumors increased (**Figure 2D** and **2E**). Furthermore, Kaplan-Meier analysis showed that high ENO3 levels in patients with ccRCC would cause a poor prognosis (**Figure 2F**). Furthermore, the clinicopathological factors of ENO3 mRNA expression level associated markedly with the TNM stage and size of the

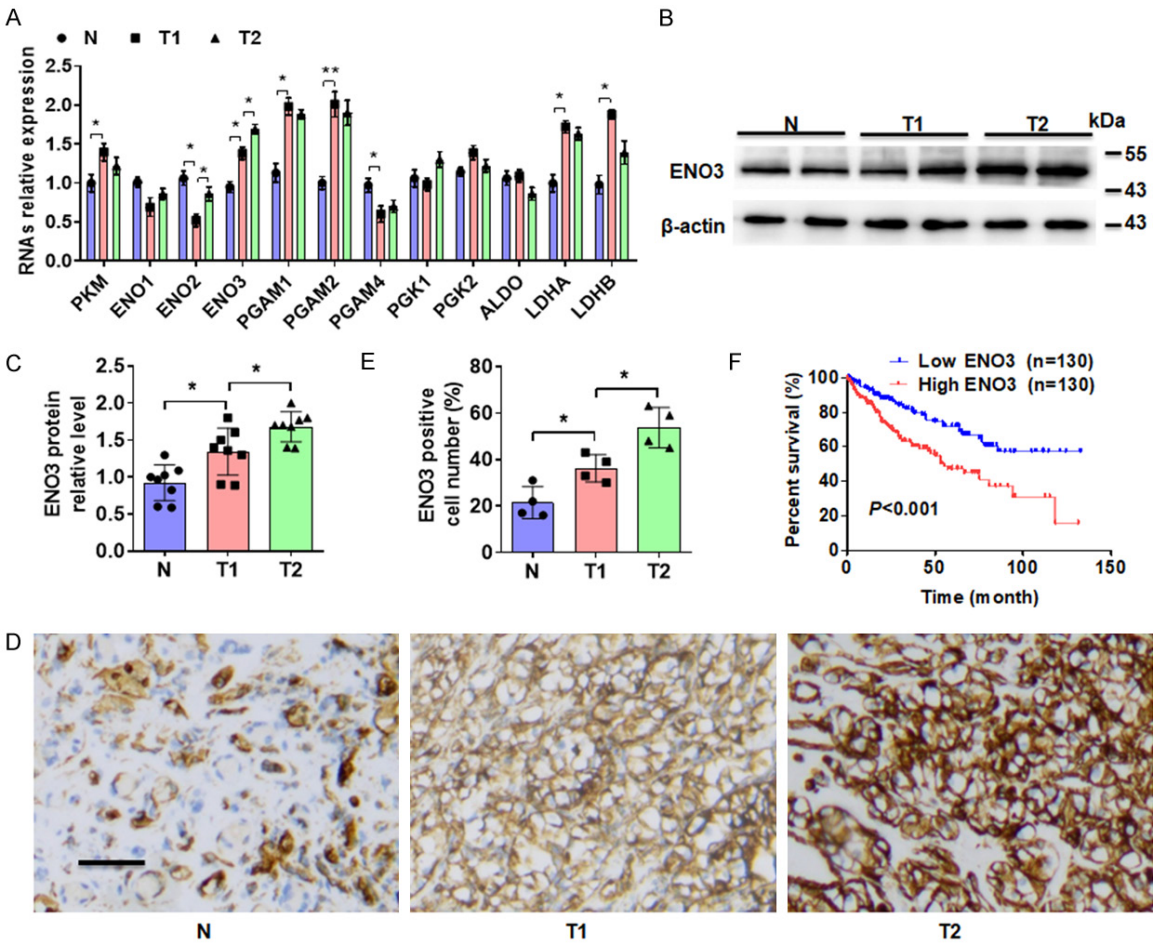

Figure 2. ENO3 (enolase 3) expression increases in ccRCC (clear cell renal cell carcinoma) tissues and leads to a poor prognosis. (A) Expression of candidate genes involved in the Warburg effect was evaluated by performing RT-qPCR (real-time quantitative polymerase chain reaction) for kidney tissue of different sizes. (B and C) Western blotting (B) or RT-qPCR (real-time quantitative polymerase chain reaction) (C) was used to determine ENO3 (enolase 3) expression in normal or kidney tissue of different sizes. (D) Immunohistochemical staining was used to determine ENO3 (enolase 3) expression in normal or kidney tissues of different sizes. Scale bar, 25 μm. (E) Quantitative analysis of the number of ENO3 (enolase 3)-positive cells in (D). (F) Kaplan-Meier analysis was used to analyze the survival of patients with ccRCC (clear cell renal cell carcinoma) using The Cancer Genome Atlas data of patients with low (n = 130) and high (n = 130) ENO3 (enolase 3) levels (http://www.oncolnc.org/). Data are expressed as mean ± standard error of the mean from three independent experiments. *P < 0.05, **P < 0.01 vs. corresponding controls.

tumors but not with age, sex, tumor size, etc. (**Table 1**). Altogether, these data support the fact that ENO3 upregulation is involved in ccRCC progression.

ENO3 upregulation promotes cell growth and enhances the Warburg effect

ENO3 expression in different ccRCC cell lines was investigated to study the function of ENO3. Results showed that ENO3 expression levels were high in A498 and 786-0 cells and low in Caki-1 cells (**Figure 3A-C**). Next, ENO3 was knocked down in 786-0 cells but overexpressed in Caki-1 cells. ENO3 depletion in 786-0 cells confirmed that both shENO3 vectors effectively downregulated *ENO3* expression, whereas *ENO3* overexpression enhanced ENO3 and mRNA levels in Caki-1 cells (**Figure 3D-F**). The MTS assay was performed to measure cell viability. As shown in **Figure 3G**, ENO3 depletion significantly reduced 786-0 cell proliferation, whereas its overexpression promoted Caki-1 cell growth. Subsequently, the Warburg effect-related function of ENO3 was explored in ccRCC cells. Results showed that ENO3 depletion reduced glucose uptake and lactic acid production, whereas its overexpression enhanced

Table 1. Clinicopathological characteristics

Characteristics	No. patients (%)	ENO3 expression		
		Low (%)	High (%)	*P* value
No. of patients	49	24	25	
Age				
≤ 58	25	13 (52.00)	12 (48.00)	0.778
> 58	24	11 (45.83)	13 (54.17)	
Gender				
Male	35	18 (51.43)	17 (48.57)	0.754
Female	14	6 (42.86)	8 (57.14)	
Tumor size (cm)				
< 5	21	15 (71.43)	6 (28.57)	0.013
≥ 5	28	10 (35.71)	18 (64.29)	
pT status				
pT_1-pT_2	21	13 (61.90)	8 (38.10)	0.283
pT_3-pT_4	28	13 (46.43)	15 (53.57)	
pN status				
pN0	30	14 (46.67)	16 (53.33)	0.962
pN1-pN3	19	9 (47.37)	10 (52.63)	
TNM stage				
I-II	23	16 (69.57)	7 (30.43)	0.022
III-IV	26	9 (34.62)	17 (65.38)	

pT: pathological Tumor; pN: pathological Node; TNM: Tumor Node Metastasis.

these effects (**Figure 3H** and **3I**). Consistent with this, ENO3 knockdown decreased, but its overexpression increased ECAR in RCC cells (**Figure 3J**). Collectively, these data established that ENO3 promotes cell proliferation by enhancing the Warburg effect.

NSUN5-mediated m5C modification of mRNA upregulates ENO3 expression

A previous study showed that m5C modification enhances gene expression by stabilizing mRNAs [38], and we investigated ENO3 upregulation in ccRCC tissues by increasing the m5C modification of mRNA. MeRIP-qPCR was performed, and m5C modification of ENO3 mRNA was increased in ccRCC tissues compared with normal renal tissues (**Figure 4A**). In parallel, m5C modification status of cell lines were examined. It was observed that 786-0 cells with high ENO3 expression had higher m5C modification levels, whereas Caki-1 cells had lower m5C modification levels (**Figure 4B**). To identify which genes participated in the m5C modification of ENO3 mRNA, the candidate m5C methyltransferase was examined in these cell lines. We found that *NSUN2*, *NSUN5*, *NSUN7*, and Tet methylcytosine dioxygenase 2 (*TET2*) had abnormal expression in different cell lines (**Figure 4C**). We knocked down these genes and detected ENO3 expression using RT-qPCR. The results showed that only NSUN5 depletion reduced ENO3 expression (**Figure 4D**). MeRIP-qPCR results also confirmed that NSUN5 depletion decreased the m5C modification levels in ENO3 mRNA (**Figure 4E**). Subsequently, the expression of NSUN5 mRNA and protein was evaluated in ccRCC tissues, and NSUN5 expression increased significantly in ccRCC tissues compared with normal renal tissues (**Figure 4F** and **4G**). Notably, the high NSUN5 expression level predicted the poor prognosis for patients with ccRCC (**Figure 4H**). Correlation analysis showed that ENO3 correlated positively with NSUN5 expression in ccRCC tissue specimens (**Figure 4I**). Furthermore, the results of double immunofluorescence staining showed that NSUN5 overexpression significantly increased the intracellular fluorescence intensity of NSUN5 and ENO3, indicating that NSUN5 and ENO3 were co-expressed in cells (**Figure 4J** and **4K**). These data revealed that m5C modification of ENO3 mRNA increases when NSUN5 expression is upregulated in ccRCC tissues and may participate in tumor progression.

NSUN5-regulated m5C modification promotes ENO3 expression by stabilizing mRNA

To investigate how NSUN5 regulates ENO3 expression, NSUN5 expression in cells was altered using short hairpin RNAs (shRNAs) or overexpression vectors. As shown in **Figure 5A-C**, 786-0 cells transfected with shNSUN5 vectors showed markedly reduced ENO3 mRNA and protein levels, whereas NSUN5 overexpression increased ENO3 expression. As expected, NSUN5 depletion decreased the ENO3 protein level, whereas NSUN5 overexpression increased it. Furthermore, cells were transfected with shRNAs or overexpression vectors and exposed to actinomycin D. RT-qPCR

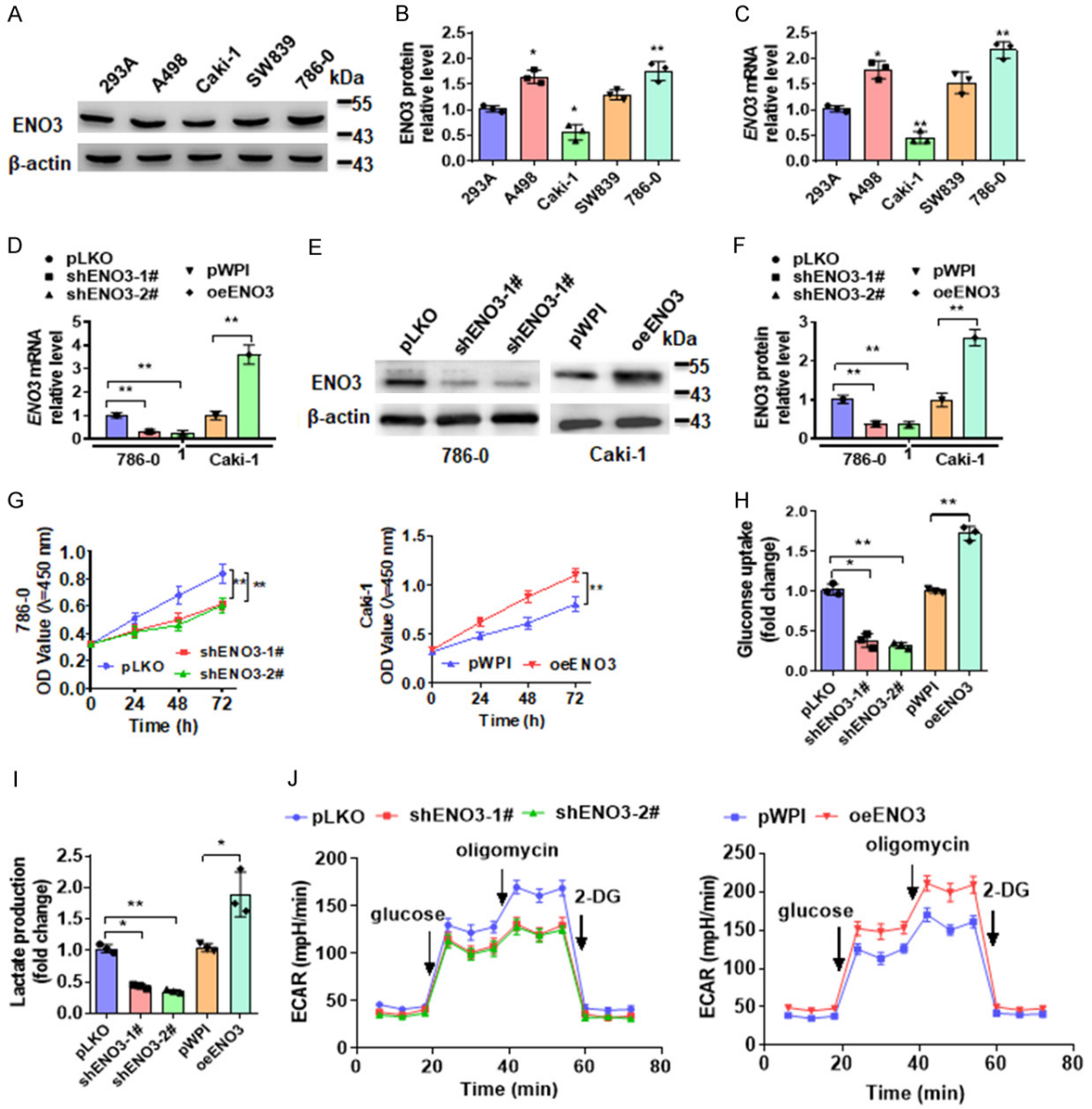

Figure 3. ENO3 (enolase 3) upregulation enhances the Warburg effect in ccRCC (clear cell renal cell carcinoma) cell lines. (A) Western blotting was used to determine ENO3 (enolase 3) expression in 293A or different renal tumor cell lines (A498, Caki-1, SW839, and 786-0 cells). (B) Quantitative analysis of protein levels. (C) ENO3 (enolase 3) mRNA expression was measured in the cell lines via RT-qPCR (real-time quantitative polymerase chain reaction). (D-F) Two shRNAs (short hairpin RNAs) targeting ENO3 (enolase 3) or overexpression vectors of ENO3 (enolase 3) were transfected into 786-0 or Caki-1 cells. RT-qPCR (real-time quantitative polymerase chain reaction) (D) or Western blotting (E and F) was used to determine ENO3 (enolase 3) expression. (G) 786-0 or Caki-1 cells were transfected as described in (D). MTS (3-(4,5-dimethylthiazol-2-yl)-5-(3-carboxymethoxyphenyl)-2-(4-sulfophenyl)-2H-tetrazolium) assay was used to investigate cell viability. (H-J) 786-0 or Caki-1 cells were treated as described in (D). Glucose uptake (H), lactic acid production (I), or ECAR (extracellular acidification rate) (J) analyses were used to evaluate the Warburg effect. Data are expressed as mean ± standard error of the mean from three independent experiments. *P < 0.05, **P < 0.01 vs. the corresponding controls.

was used to detect ENO3 mRNA stability. The results showed that NSUN5 depletion significantly reduced ENO3 mRNA levels after actinomycin D-mediated stimulation. In contrast, NSUN5 overexpression enhanced ENO3 mRNA stability (**Figure 5D**). Additionally, MeRIP-qPCR results confirmed that NSUN5 depletion reduced m5C-modified ENO3 mRNA levels, whereas NSUN5 overexpression increased them (**Figure 5E**). Altogether, these results con-

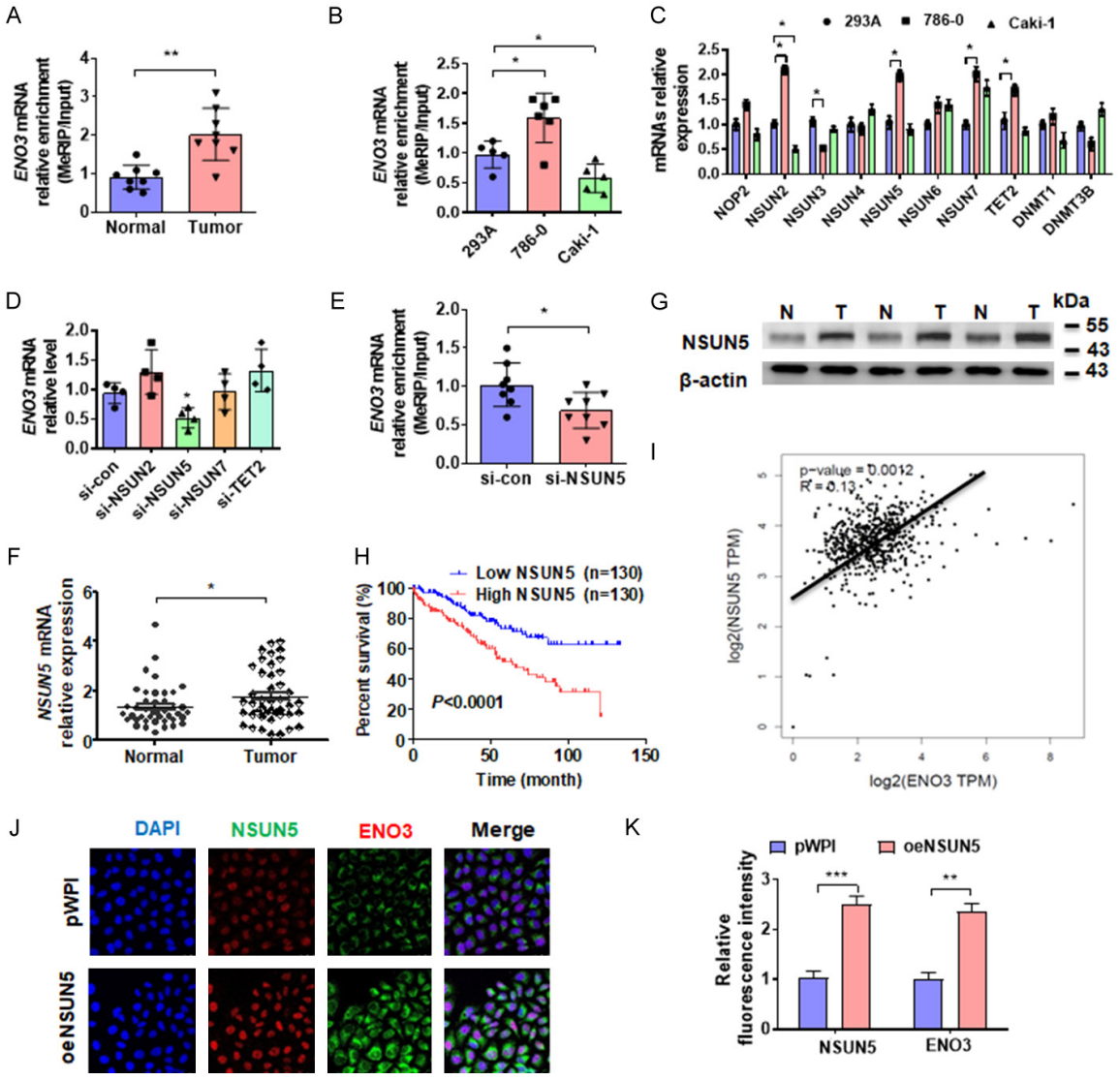

Figure 4. NSUN5 (NOP2/Sun RNA methyltransferase 5)-mediated m5C (5-methylcytosine) modification of mRNA upregulates ENO3 (enolase 3) expression. A. Total RNA from normal and RCC (renal cell carcinoma) tissues were extracted, and MeRIP-qPCR (m5C RNA immunoprecipitation-quantitative polymerase chain reaction) was used to detect ENO3 (enolase 3) mRNA enrichment using the m5C (5-methylcytosine) antibody. B. MeRIP-qPCR (m5C RNA immunoprecipitation-quantitative polymerase chain reaction) was used to determine m5C (5-methylcytosine) modification levels in ENO3 (enolase 3) mRNA. C. RT-qPCR (real-time quantitative polymerase chain reaction) was performed to detect the candidate genes of m5C (5-methylcytosine) methyltransferase in 293A, 786-0, or Caki-1 cells. D. Genes were knocked down in 786-0 cells, and RT-qPCR (real-time quantitative polymerase chain reaction) was used to determine ENO3 (enolase 3) mRNA expression. E. 786-0 cells were transfected with si-NSUN5 (small interfering-NOP2/Sun RNA methyltransferase 5) or control siRNA (small interfering RNA), and then MeRIP-qPCR (m5C RNA immunoprecipitation-quantitative polymerase chain reaction) was used to detect ENO3 (enolase 3) mRNA enrichment using the m5C (5-methylcytosine) antibody. F and G. NSUN5 (NOP2/Sun RNA methyltransferase 5) mRNA or protein levels in RCC (renal cell carcinoma) or normal kidney tissues were measured using RT-qPCR (real-time quantitative polymerase chain reaction) and Western blotting. H. Kaplan-Meier analysis was used to analyze the survival of patients with ccRCC (clear cell renal cell carcinoma) using The Cancer Genome Atlas data of patients with low (n = 130) and high (n = 130) NSUN5 (NOP2/Sun RNA methyltransferase 5) levels (http://www.oncolnc.org/). I. Correlation analysis (Gene Expression Profiling Interactive Analysis; http://gepia.cancer-pku.cn/) revealed a positive correlation between ENO3 (enolase 3) and NSUN5 (NOP2/Sun RNA methyltransferase 5) in ccRCC tissues. J and K. Caki-1 cells were infected with oeNSUN5 (overexpression NOP2/Sun RNA methyltransferase 5) or pWPI vector, and then double immunofluorescence was used to detect ENO3 (enolase 3) and NSUN5 (NOP2/Sun RNA methyltransferase 5) co-expression. Scale bar, 20 μm. Data are expressed as mean ± standard deviation. *P < 0.05, **P < 0.01 vs. corresponding controls.

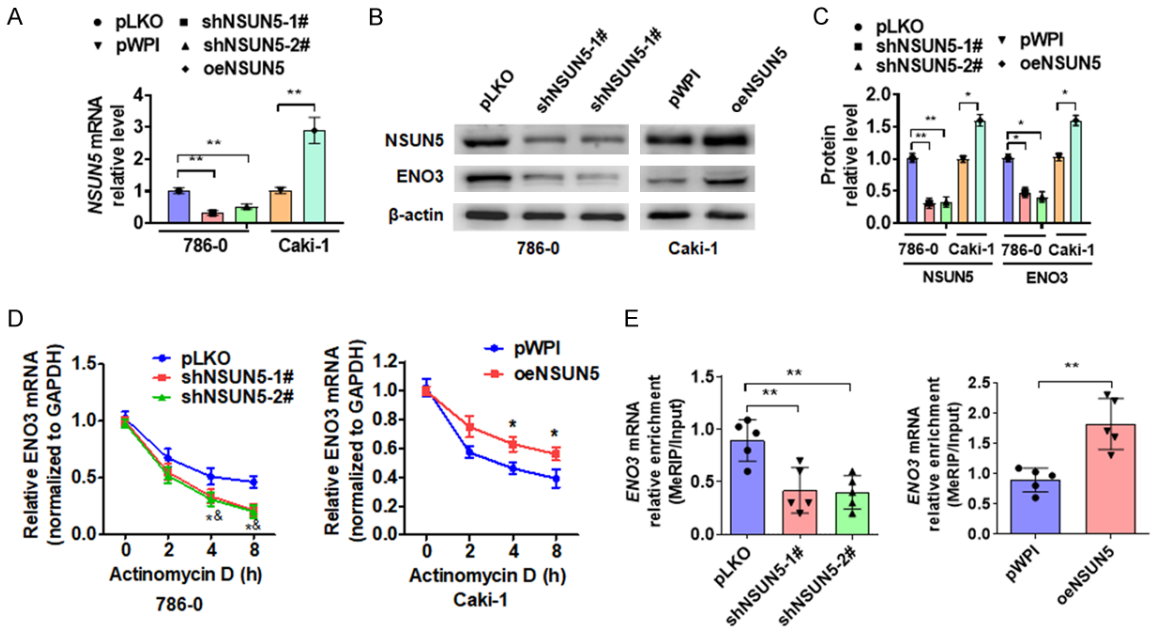

Figure 5. m5C (5-methylcytosine) modification enhances ENO3 (enolase 3) mRNA stability. (A-C) 786-0 cells were transfected with shNSUN5-1# (short hairpin RNAs NOP2/Sun RNA methyltransferase 5-1), shNSUN5-2# (short hairpin RNAs NOP2/Sun RNA methyltransferase 5-2), or control vector (pLKO), and Caki-1 cells were infected with oeNSUN5 (overexpression NOP2/Sun RNA methyltransferase 5) or pWPI vector. RT-qPCR (real-time quantitative polymerase chain reaction) (A) or Western blotting (B and C) was used to determine NSUN5 (NOP2/Sun RNA methyltransferase 5) expression. (D) Cells were transfected as described in (A) and exposed to actinomycin D for zero, two, four, and eight hours. NSUN5 (NOP2/Sun RNA methyltransferase 5) mRNA levels were measured using RT-qPCR (real-time quantitative polymerase chain reaction). (E) MeRIP-qPCR (m5C RNA immunoprecipitation-quantitative polymerase chain reaction) was used to determine m5C (5-methylcytosine)-modified ENO3 (enolase 3) mRNA levels after NSUN5 (NOP2/Sun RNA methyltransferase 5) knockdown or overexpression. Data are expressed as mean ± standard deviation. *P < 0.05, **P < 0.01 vs. corresponding controls.

firm that NSUN5 promotes m5C modification of mRNA and ENO3 expression via mRNA stabilization.

NSUN5 is involved in the ENO3-regulated Warburg effect

Rescue experiments were performed to determine whether NSUN5 participates in the ENO3-regulated Warburg effect. 786-0 cells were transfected with shNSUN5, shENO3, or both, and glucose uptake and lactic acid production assays were performed. Results showed that NSUN5 depletion significantly reduced the glucose uptake and lactic acid production rates, which were enhanced when knocked down together (**Figure 6A** and **6C**). Conversely, NSUN5 overexpression increased the glucose uptake and lactic acid production rates, whereas ENO3 knockdown reduced these effects (**Figure 6B** and **6D**). Consistent with these findings, the ECAR assay also revealed similar results (**Figure 6E** and **6F**). NSUN5 depletion reduced cell viability, whereas ENO3 knockdown increased it (**Figure 6G**). Conversely, NSUN5 overexpression promoted cell viability, and ENO3 depletion simultaneously decreased these effects (**Figure 6H**). These results indicated that the NSUN5/ENO3 axis regulates the Warburg effect and promotes ccRCC progression.

Blocking the NSUN5/ENO3 axis inhibits ccRCC progression in vivo

To investigate whether the NSUN5/ENO3 axis disruption inhibits xenograft progression, NSUN5, ENO3, or both were stably knocked down in 786-0 cells using a lentivirus. As shown in **Figure 7A**, ENO3 or NSUN5 depletion caused small tumors that control vectors, but their combined knockdown enhanced these effects. Consistent with this, ENO3 or NSUN5 depletion resulted in tumors having a small size or low wet weight, whereas the depletion of both simultaneously reduced the tumor size or wet

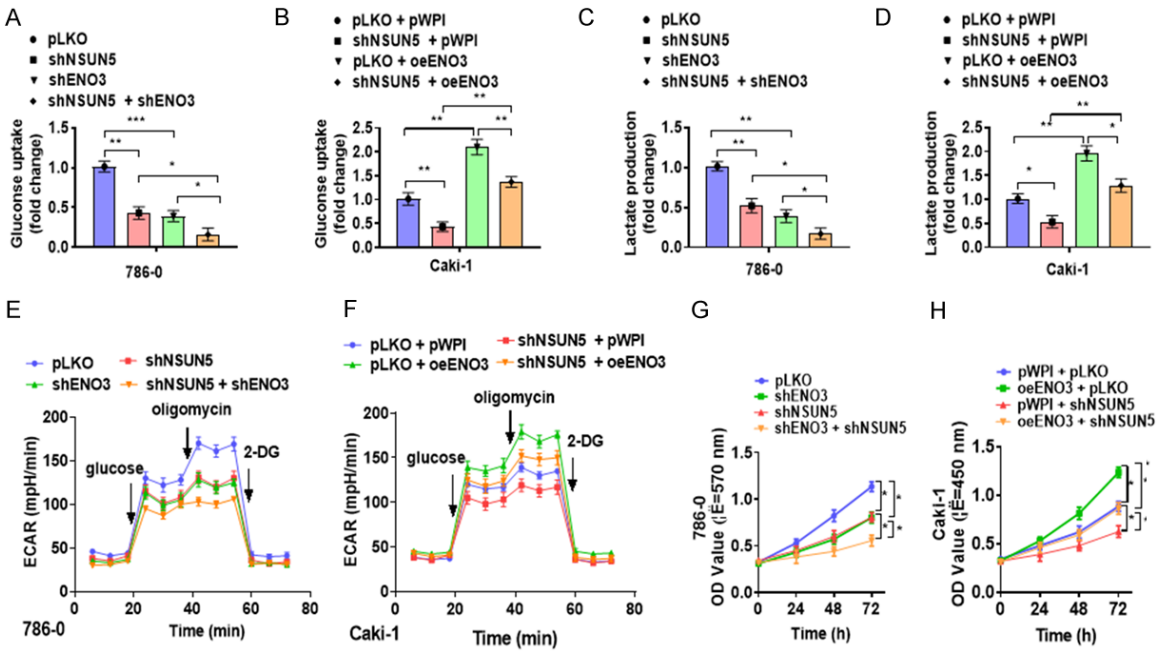

Figure 6. NSUN5 (NOP2/Sun RNA methyltransferase 5) is involved in the ENO3 (enolase 3)-regulated Warburg effect in ccRCC (clear cell renal cell carcinoma) cell lines. (A) 786-0 cells were transfected with shNSUN5 (short hairpin RNAs NOP2/Sun RNA methyltransferase 5), shENO3 (short hairpin enolase 3), or both vectors simultaneously, and glucose uptake analysis was used to evaluate glucose consumption in cells. (B) Caki-1 cells were transfected with shNSUN5 (short hairpin RNAs NOP2/Sun RNA methyltransferase 5), oeENO3 (overexpression enolase 3), or both vectors simultaneously, and glucose uptake analysis was used to evaluate glucose consumption in cells. (C and D) Lactic acid production analysis was used to determine the amount of lactic acid produced in kidney cells after the indicated transfection. (E and F) 786-0 and Caki-1 cells were transfected as described above, and ECAR (extracellular acidification rate) test was used to analyze the extracellular acidification efficiency of cells. (G and H) Cells were transfected as described in (A) or (B), and the MTS (3-(4,5-dimethylthiazol-2-yl)-5-(3-carboxymethoxyphenyl)-2-(4-sulfophenyl)-2H-tetrazolium) assay was used to determine cell viability. Data are expressed as mean ± standard deviation. *P < 0.05, **P < 0.01 vs. corresponding controls.

weight (**Figure 7B** and **7C**). Western blotting demonstrated that NSUN5 depletion inhibited ENO3 and CDK6 expression, but their expression was enhanced when depleted together (**Figure 7D** and **7E**). Additionally, double immunofluorescence staining of tumor tissues confirmed these results (**Figure 7F**). Altogether, the results revealed that the NSUN5/ENO3 axis disruption inhibits tumor progression in the xenograft model, and the inhibition of the NSUN5/ENO3 axis-regulated Warburg effect may be a potential therapeutic strategy for ccRCC treatment.

Discussion

Metabolic changes are particularly prominent in renal cancer, especially in ccRCC, the most common and fatal subtype of human renal cancer [39]. Due to extensive metabolic changes, ccRCC is described as a "cell metabolism disease" [40]. To promote growth, survival, proliferation, and long-term maintenance, ccRCC cells often reprogram their metabolism [41]. The most common of these reprogramming are increased glucose uptake and fermentation of glucose to lactic acid. This type of aerobic glycolysis occurs even under aerobic conditions as well as in the presence of intact mitochondria and is called the Warburg effect [9]. Compared to oxidative phosphorylation, the Warburg effect is inefficient in ATP production [42]. However, renal cancer cells switch to aerobic glycolysis to grow faster and compete for energy [41]. The amount of ATP required for cell growth and proliferation seems to be much lower than that required for cell maintenance and survival [43]. That is why increased glucose metabolism supports anabolism and cell proliferation throughout nature. Therefore, the Warburg effect in larger tumors is often enhanced to obtain more cell proliferation and

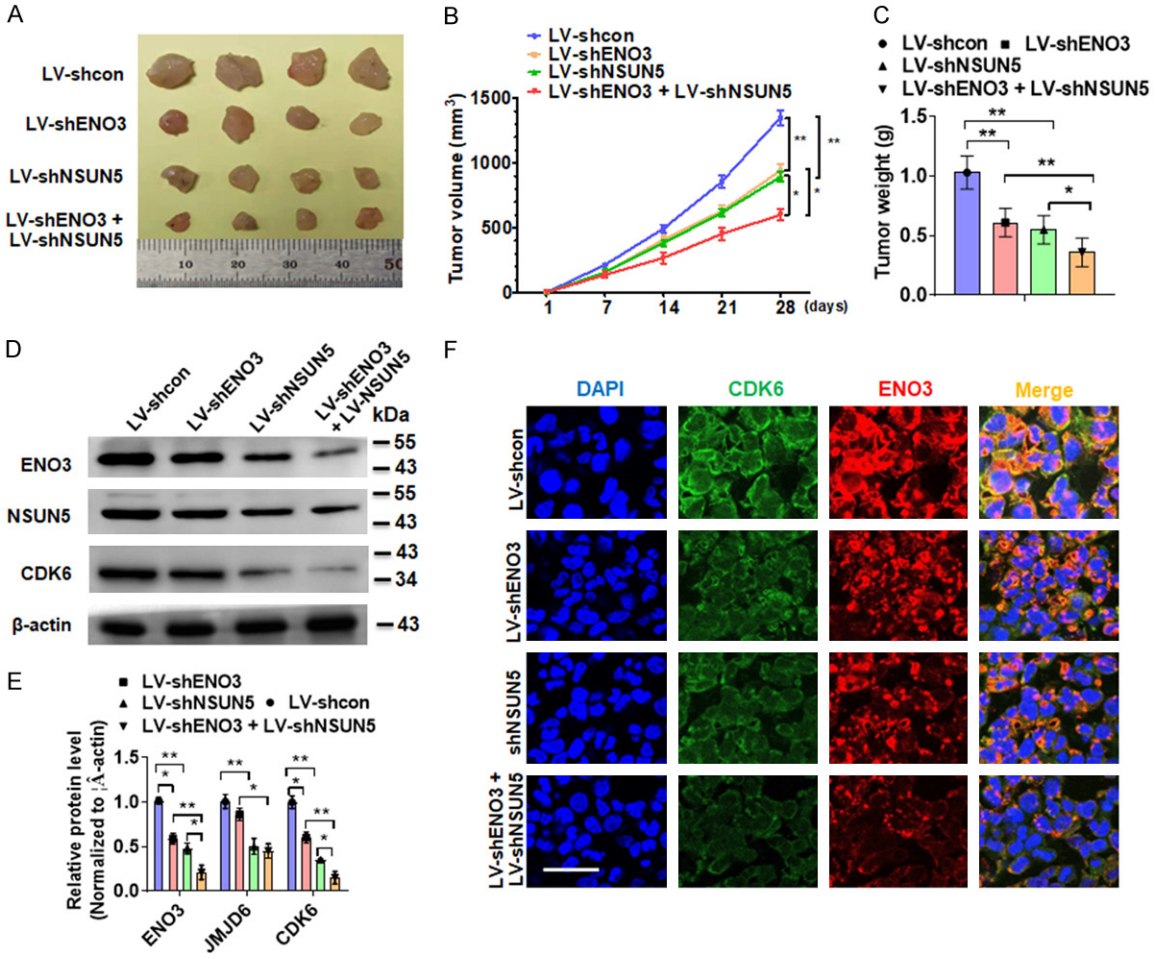

Figure 7. Inhibition of NSUN5 (NOP2/Sun RNA methyltransferase 5)-mediated m5C (5-methylcytosine) modification of ENO3 (enolase 3) mRNA inhibits ccRCC (clear cell renal cell carcinoma) progression *in vivo*. (A) *ENO3* (enolase 3), *NSUN5* (NOP2/Sun RNA methyltransferase 5), or both were stably depleted simultaneously in 786-0 cells and injected into nude mice to construct ccRCC (clear cell renal cell carcinoma) xenograft cancer models. Tumor volumes were measured directly. (B) Tumor sizes in each group of mice. (C) The wet weight of xenograft tumors of each mice group was analyzed. (D) ENO3 (enolase 3), NSUN5 (NOP2/Sun RNA methyltransferase 5), and CDK6 (Cyclin-Dependent Kinases 6) levels were determined via Western blotting of xenograft tumors. (E) Quantitative analysis of (D). (F) Double immunofluorescence staining was used to determine CDK6 (Cyclin-Dependent Kinases 6) and ENO3 (enolase 3) expression in xenograft tumor tissues. Scale bar, 25 μm. Data are expressed as mean ± standard deviation. *P < 0.05, **P < 0.01 vs. the corresponding controls.

migration resources. In this study, cells obtained from larger tumors exhibited a stronger Warburg effect than cells obtained from small tumors. The theoretical evolutionary game theory supports the fact that cells with higher ATP productivity but lower yield may gain a selective advantage when competing for shared and limited energy resources [44, 45].

As a 2-phospho-D-glycerate hydrolase, ENO participates in the glycolysis pathway and catalyzes the dehydration of 2-phospho-D-glyceric acid to phosphoenolpyruvate [17, 46]. Studies have reported that ENO participates in the Warburg effect during the development of various tumors [41]. ENO1 knockdown targets the Warburg effect in cancer cells to increase oxidative phosphorylation and induce growth arrest [47]. Type 1 transmembrane glycoprotein B7-H3 interacts with ENO1 to promote HeLa cell progression [48]. ENO3 knockdown can inhibit the proliferation of lung cancer with STK11 mutations and show selective anticancer effects [23]. Low ENO2 and ENO3 expression associate significantly with longer overall survival of patients with colorectal cancer [24].

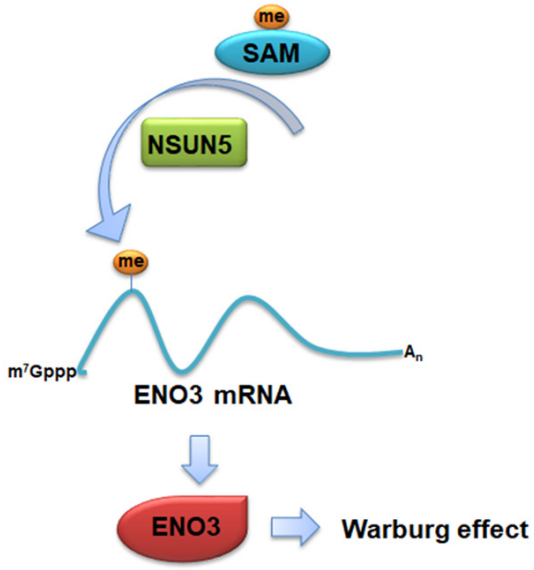

Figure 8. Proposed model for the NSUN5 (NOP2/Sun RNA methyltransferase 5)/ENO3 (enolase 3) axis-meditated regulation of the Warburg effect in ccRCC (clear cell renal cell carcinoma) cells.

However, the expression and function of ENO3 in ccRCC remain unclear. In this study, ENO3 was upregulated in ccRCC cells. ENO3 increased with an increase in ccRCC tumor size. Furthermore, high levels of ENO3 indicated a poor prognosis for patients. Cell function studies showed that ENO3 promotes cell growth and enhances the Warburg effect (**Figure 8**).

With technological advancements, such as gene sequencing, RNA modification plays an play an important role in gene expression [49]. Among them, m5C modification is a common and high-content RNA modification. m5C-modified RNAs include ribosomal RNA, transfer RNA, mRNA, enhancer RNA, and several non-coding RNAs [50]. Generally, the NOL1/NOP2/SUN domain family of enzymes (e.g., NSUN) and the DNA methyltransferase homolog DNMT2 catalyzes the regulation of m5C modification [51]. Many studies have shown that m5C modification of RNA mediated by the NSUN family is closely related to tumor occurrence and development [52]. NSUN2 promotes gastric cancer cell proliferation by inhibiting $p57^{Kip2}$ expression in an m5C-dependent manner [53]. NSUN2-regulated m5C modification promotes bladder cancer pathogenesis via mRNA stabilization [38]. This study investigated the m5C methyltransferase in RCC cell lines and found that NSUN2, NSUN5, NSUN7, and TET2 were abnormally expressed in different cell lines. However, only NSUN5 depletion reduced ENO3 expression. Furthermore, NSUN5 was upregulated in ccRCC clinical samples, and high NSUN5 levels indicated a poor prognosis for patients with ccRCC. NSUN5 upregulation promoted mRNA stability and ENO3 expression by mediating m5C modification. Also, NSUN5 was related to Williams-Beuren syndrome and cell senescence [54, 55].

Cyclin-Dependent Kinases 6 (CDK6) is a cell cycle kinase whose main function is to regulate the cell proliferation cycle [56]. Recently, CDK6 has been widely used in the study of the cancer cell cycle. Reducing CDK6 expression significantly inhibited tumor cell Rb/E2F export, which then regulates tumor cell growth [57]. In acute myeloid leukemia, CDK6 expression is markedly increased, and CDK6 knockdown can attenuate the effect of the NUP98 fusion protein and improve the prognosis of acute myeloid leukemia [58]. lnc-UCID binds to DHX9, thereby weakening the inhibitory effect of DHX9 on CDK6, enhancing CDK6 expression, and further promoting the transformation of cells in the G1/S phase and the proliferation of hepatoma cells [59]. Additionally, YAP improves the premature aging of cells and cognitive decline in patients with Alzheimer's disease by promoting CDK6 expression [60]. In our study, we used CDK6 to represent the proliferation of ccRCC cells. Our results indicate that a decrease in NSUN5 and ENO3 expression inhibits the CDK6 level and slow ccRCC tumor growth.

ccRCCs have high immune infiltration and are significantly affected by tumor metabolism and microenvironment [61]. Currently, the research on the metabolism and microenvironment of ccRCCs remains the focus. Some researchers have improved the possibility of targeted therapy for ccRCCs through single-cell sequencing, but this also has some inevitable drawbacks, such as huge costs [62]. In our study, we focused on the metabolism of cancer. Firstly, primary cells from ccRCC tissues were isolated and cultured, and cells from large tumors were observed to have a stronger Warburg effect than the small ones. ENO3 was involved in the Warburg effect with the tumor size increase in ccRCC, and a high level of ENO3 predicted a poor prognosis for patients. A cell function

study revealed that ENO3 promoted cell growth and enhanced the Warburg effect. In this study, NSUN5 upregulation promoted mRNA stability and ENO3 expression by mediating mRNA 5-methylcytosine (m5C) in ccRCC. The finding revealed that NSUN5/ENO3 axis plays a critical role in ccRCC progression and may serve as a potential therapeutic target. Undoubtedly, our research needs to be further in-depth. Moving forward, we will study how NSUN5/ENO3 regulates CDK6 expression to regulate tumor proliferation, which will elucidate the mechanism of tumor metabolism affecting tumor growth in more detail.

Conclusion

This study found that large ccRCC tumors exhibit a stronger Warburg effect. ENO3 upregulation is implicated in the Warburg effect and further promotes ccRCC cell growth. High NSUN5 expression promotes mRNA stability and ENO3 expression by mediating m5C modification of mRNA in ccRCC cells. These data provide theoretical evidence that the NSUN5/ENO3 axis plays a critical role in ccRCC progression. Therefore, a comprehensive understanding of the mechanisms regulating the NSUN5/ENO3 axis will promote the development of effective therapeutic strategies against ccRCC progression.

Acknowledgements

This study was partially supported by Hebei Science and Technology Department (16967796D).

All experimental protocols were reviewed and approved by the Ethics Committee of the Second Hospital of Hebei Medical University (No. 2018-R131). In addition, the animal study was approved by the Ethics Committee of the Second Hospital of Hebei Medical University with the approval number of No. 2018-AE035. The patients/guardians provided written informed consent for tumor studies.

Disclosure of conflict of interest

None.

Abbreviations

ccRCC, clear cell Renal Cell Carcinoma; ECAR, Extracellular Acidification Rate; ENO3, Enolase 3; MeRIP-qPCR, m5C RNA immunoprecipitation-quantitative Polymerase Chain Reaction; m5C, 5-methylcytosine; MFI, Microflow Imaging; mRNA, messenger RNA; MTS, 3-(4, 5-dimethylthiazol-2-yl)-5-(3-carboxymethoxyphenyl)-2-(4-sulfophenyl)-2H-tetrazolium; NSUN5, NOP2/Sun RNA methyltransferase 5; RT-qPCR, Real-Time quantitative Polymerase Chain Reaction; shRNAs, short hairpin RNAs; CDK6, Cyclin-Dependent Kinases 6; RPMI, Roswell Park Memorial Institute; BP-Flex, Bioprofile Flex analyzer; FBS, Fetal Bovine Serum.

Address correspondence to: Yue-Heng Wang, Department of Cardiac Ultrasound, The Second Hospital of Hebei Medical University, 215 Heping West Road, Shijiazhuang 050000, Hebei, China. Tel: +86-311-6600-3733; Fax: +86-311-6600-3733; E-mail: wyh5766@163.com

References

[1] Gray RE and Harris GT. Renal cell carcinoma: diagnosis and management. Am Fam Physician 2019; 99: 179-184.

[2] Chen W, Zheng R, Baade PD, Zhang S, Zeng H, Bray F, Jemal A, Yu XQ and He J. Cancer statistics in China, 2015. CA Cancer J Clin 2016; 66: 115-132.

[3] Padala SA and Kallam A. Clear cell renal carcinoma. StatPearls: Treasure Island (FL); 2022.

[4] Deleuze A, Saout J, Dugay F, Peyronnet B, Mathieu R, Verhoest G, Bensalah K, Crouzet L, Laguerre B, Belaud-Rotureau MA, Rioux-Leclercq N and Kammerer-Jacquet SF. Immunotherapy in renal cell carcinoma: the future is now. Int J Mol Sci 2020; 21: 2532.

[5] Bedke J, Gauler T, Grunwald V, Hegele A, Herrmann E, Hinz S, Janssen J, Schmitz S, Schostak M, Tesch H, Zastrow S and Miller K. Systemic therapy in metastatic renal cell carcinoma. World J Urol 2017; 35: 179-188.

[6] Choueiri TK, Escudier B, Powles T, Mainwaring PN, Rini BI, Donskov F, Hammers H, Hutson TE, Lee JL, Peltola K, Roth BJ, Bjarnason GA, Geczi L, Keam B, Maroto P, Heng DY, Schmidinger M, Kantoff PW, Borgman-Hagey A, Hessel C, Scheffold C, Schwab GM, Tannir NM and Motzer RJ; METEOR Investigators. Cabozantinib versus everolimus in advanced renal-cell carcinoma. N Engl J Med 2015; 373: 1814-1823.

[7] Li X, Hou G, Zhu Z, Yan F, Wang F, Wei D, Zheng Y, Yuan J, Zheng W, Zhang G, Meng P, Guo Y, Li X, Yao L, Shen L and Yuan J. The tumor suppressor NDRG2 cooperates with an mTORC1 inhibitor to suppress the Warburg effect in re-

nal cell carcinoma. Invest New Drugs 2020; 38: 956-966.
[8] Linehan WM, Srinivasan R and Schmidt LS. The genetic basis of kidney cancer: a metabolic disease. Nat Rev Urol 2010; 7: 277-285.
[9] Liberti MV and Locasale JW. The Warburg effect: how does it benefit cancer cells? Trends Biochem Sci 2016; 41: 211-218.
[10] Warburg O. On the origin of cancer cells. Science 1956; 123: 309-314.
[11] Yuen CA, Asuthkar S, Guda MR, Tsung AJ and Velpula KK. Cancer stem cell molecular reprogramming of the Warburg effect in glioblastomas: a new target gleaned from an old concept. CNS Oncol 2016; 5: 101-108.
[12] Taniguchi K, Sakai M, Sugito N, Kumazaki M, Shinohara H, Yamada N, Nakayama T, Ueda H, Nakagawa Y, Ito Y, Futamura M, Uno B, Otsuki Y, Yoshida K, Uchiyama K and Akao Y. PTBP1-associated microRNA-1 and -133b suppress the Warburg effect in colorectal tumors. Oncotarget 2016; 7: 18940-18952.
[13] Yao Z, Zhang Q, Guo F, Guo S, Yang B, Liu B, Li P, Li J, Guan S and Liu X. Long noncoding RNA PCED1B-AS1 promotes the Warburg effect and tumorigenesis by upregulating HIF-1alpha in glioblastoma. Cell Transplant 2020; 29: 963689720906777.
[14] Shamsi M, Saghafian M, Dejam M and Sanati-Nezhad A. Mathematical modeling of the function of Warburg effect in tumor microenvironment. Sci Rep 2018; 8: 8903.
[15] Soltysova A, Breza J, Takacova M, Feruszova J, Hudecova S, Novotna B, Rozborilova E, Pastorekova S, Kadasi L and Krizanova O. Deregulation of energetic metabolism in the clear cell renal cell carcinoma: a multiple pathway analysis based on microarray profiling. Int J Oncol 2015; 47: 287-295.
[16] Lim HY, Yip YM, Chiong E, Tiong HY, Halliwell B, Esuvaranathan K and Wong KP. Metabolic signatures of renal cell carcinoma. Biochem Biophys Res Commun 2015; 460: 938-943.
[17] Huang H, Tang S, Ji M, Tang Z, Shimada M, Liu X, Qi S, Locasale JW, Roeder RG, Zhao Y and Li X. p300-mediated lysine 2-hydroxyisobutyrylation regulates glycolysis. Mol Cell 2018; 70: 663-678, e6.
[18] Lopez-Alemany R, Longstaff C, Hawley S, Mirshahi M, Fabregas P, Jardi M, Merton E, Miles LA and Felez J. Inhibition of cell surface mediated plasminogen activation by a monoclonal antibody against alpha-enolase. Am J Hematol 2003; 72: 234-242.
[19] Xu CM, Luo YL, Li S, Li ZX, Jiang L, Zhang GX, Owusu L and Chen HL. Multifunctional neuron-specific enolase: its role in lung diseases. Biosci Rep 2019; 39: BSR20192732.
[20] Muoio B, Pascale M and Roggero E. The role of serum neuron-specific enolase in patients with prostate cancer: a systematic review of the recent literature. Int J Biol Markers 2018; 33: 10-21.
[21] Isgro MA, Bottoni P and Scatena R. Neuron-specific enolase as a biomarker: biochemical and clinical aspects. Adv Exp Med Biol 2015; 867: 125-143.
[22] Ho JA, Chang HC, Shih NY, Wu LC, Chang YF, Chen CC and Chou C. Diagnostic detection of human lung cancer-associated antigen using a gold nanoparticle-based electrochemical immunosensor. Anal Chem 2010; 82: 5944-5950.
[23] Park C, Lee Y, Je S, Chang S, Kim N, Jeong E and Yoon S. Overexpression and selective anticancer efficacy of ENO3 in STK11 mutant lung cancers. Mol Cells 2019; 42: 804-809.
[24] Pan X, Wu H, Chen G and Li W. Prognostic value of enolase gene family in colon cancer. Med Sci Monit 2020; 26: e922980.
[25] Zhu J, Wang S, Bai H, Wang K, Hao J, Zhang J and Li J. Identification of five glycolysis-related gene signature and risk score model for colorectal cancer. Front Oncol 2021; 11: 588811.
[26] Kong KW, Abdul Aziz A, Razali N, Aminuddin N and Mat Junit S. Antioxidant-rich leaf extract of Barringtonia racemosa significantly alters the in vitro expression of genes encoding enzymes that are involved in methylglyoxal degradation III. PeerJ 2016; 4: e2379.
[27] Heissenberger C, Liendl L, Nagelreiter F, Gonskikh Y, Yang G, Stelzer EM, Krammer TL, Micutkova L, Vogt S, Kreil DP, Sekot G, Siena E, Poser I, Harreither E, Linder A, Ehret V, Helbich TH, Grillari-Voglauer R, Jansen-Durr P, Kos M, Polacek N, Grillari J and Schosserer M. Loss of the ribosomal RNA methyltransferase NSUN5 impairs global protein synthesis and normal growth. Nucleic Acids Res 2019; 47: 11807-11825.
[28] Jiang Z, Li S, Han MJ, Hu GM and Cheng P. High expression of NSUN5 promotes cell proliferation via cell cycle regulation in colorectal cancer. Am J Transl Res 2020; 12: 3858-3870.
[29] Wang Y, Jiang T, Xu J, Gu Y, Zhou Y, Lin Y, Wu Y, Li W, Wang C, Shen B, Mo X, Wang X, Zhou B, Ding C and Hu Z. Mutations in RNA methyltransferase gene NSUN5 confer high risk of outflow tract malformation. Front Cell Dev Biol 2021; 9: 623394.
[30] van Beers MMC, Slooten C, Meulenaar J, Sediq AS, Verrijk R and Jiskoot W. Micro-flow imaging as a quantitative tool to assess size and agglomeration of PLGA microparticles. Eur J Pharm Biopharm 2017; 117: 91-104.

[31] Tan X, Zhai Y, Chang W, Hou J, He S, Lin L, Yu Y, Xu D, Xiao J, Ma L, Wang G, Cao T and Cao G. Global analysis of metastasis-associated gene expression in primary cultures from clinical specimens of clear-cell renal-cell carcinoma. Int J Cancer 2008; 123: 1080-1088.
[32] Peng C, Hou ST, Deng CX and Zhang Y. Function of DHX33 in promoting Warburg effect via regulation of glycolytic genes. J Cell Physiol 2021; 236: 981-996.
[33] Yang Z, Qu CB, Zhang Y, Zhang WF, Wang DD, Gao CC, Ma L, Chen JS, Liu KL, Zheng B, Zhang XH, Zhang ML, Wang XL, Wen JK and Li W. Dysregulation of p53-RBM25-mediated circAMOTL1L biogenesis contributes to prostate cancer progression through the circAMOTL1L-miR-193a-5p-Pcdha pathway. Oncogene 2019; 38: 2516-2532.
[34] Yang Z, Chen JS, Wen JK, Gao HT, Zheng B, Qu CB, Liu KL, Zhang ML, Gu JF, Li JD, Zhang YP, Li W, Wang XL and Zhang Y. Silencing of miR-193a-5p increases the chemosensitivity of prostate cancer cells to docetaxel. J Exp Clin Cancer Res 2017; 36: 178.
[35] Qi JC, Yang Z, Lin T, Ma L, Wang YX, Zhang Y, Gao CC, Liu KL, Li W, Zhao AN, Shi B, Zhang H, Wang DD, Wang XL, Wen JK and Qu CB. CDK13 upregulation-induced formation of the positive feedback loop among circCDK13, miR-212-5p/miR-449a and E2F5 contributes to prostate carcinogenesis. J Exp Clin Cancer Res 2021; 40: 2.
[36] Ren LX, Qi JC, Zhao AN, Shi B, Zhang H, Wang DD and Yang Z. Myc-associated zinc-finger protein promotes clear cell renal cell carcinoma progression through transcriptional activation of the MAP2K2-dependent ERK pathway. Cancer Cell Int 2021; 21: 323.
[37] Yang Z, Zheng B, Zhang Y, He M, Zhang XH, Ma D, Zhang RN, Wu XL and Wen JK. miR-155-dependent regulation of mammalian sterile 20-like kinase 2 (MST2) coordinates inflammation, oxidative stress and proliferation in vascular smooth muscle cells. Biochim Biophys Acta 2015; 1852: 1477-1489.
[38] Chen X, Li A, Sun BF, Yang Y, Han YN, Yuan X, Chen RX, Wei WS, Liu Y, Gao CC, Chen YS, Zhang M, Ma XD, Liu ZW, Luo JH, Lyu C, Wang HL, Ma J, Zhao YL, Zhou FJ, Huang Y, Xie D and Yang YG. 5-methylcytosine promotes pathogenesis of bladder cancer through stabilizing mRNAs. Nat Cell Biol 2019; 21: 978-990.
[39] Hakimi AA, Reznik E, Lee CH, Creighton CJ, Brannon AR, Luna A, Aksoy BA, Liu EM, Shen R, Lee W, Chen Y, Stirdivant SM, Russo P, Chen YB, Tickoo SK, Reuter VE, Cheng EH, Sander C and Hsieh JJ. An integrated metabolic atlas of clear cell renal cell carcinoma. Cancer Cell 2016; 29: 104-116.
[40] Courtney KD, Bezwada D, Mashimo T, Pichumani K, Vemireddy V, Funk AM, Wimberly J, McNeil SS, Kapur P, Lotan Y, Margulis V, Cadeddu JA, Pedrosa I, DeBerardinis RJ, Malloy CR, Bachoo RM and Maher EA. Isotope tracing of human clear cell renal cell carcinomas demonstrates suppressed glucose oxidation in vivo. Cell Metab 2018; 28: 793-800, e2.
[41] Vander Heiden MG, Cantley LC and Thompson CB. Understanding the Warburg effect: the metabolic requirements of cell proliferation. Science 2009; 324: 1029-1033.
[42] Zheng J. Energy metabolism of cancer: glycolysis versus oxidative phosphorylation (Review). Oncol Lett 2012; 4: 1151-1157.
[43] Locasale JW and Cantley LC. Metabolic flux and the regulation of mammalian cell growth. Cell Metab 2011; 14: 443-451.
[44] Slavov N, Budnik BA, Schwab D, Airoldi EM and van Oudenaarden A. Constant growth rate can be supported by decreasing energy flux and increasing aerobic glycolysis. Cell Rep 2014; 7: 705-714.
[45] Pfeiffer T, Schuster S and Bonhoeffer S. Cooperation and competition in the evolution of ATP-producing pathways. Science 2001; 292: 504-507.
[46] Sugahara T, Nakajima H, Shirahata S and Murakami H. Purification and characterization of immunoglobulin production stimulating factor-II beta derived from Namalwa cells. Cytotechnology 1992; 10: 137-146.
[47] Capello M, Ferri-Borgogno S, Riganti C, Chattaragada MS, Principe M, Roux C, Zhou W, Petricoin EF, Cappello P and Novelli F. Targeting the Warburg effect in cancer cells through ENO1 knockdown rescues oxidative phosphorylation and induces growth arrest. Oncotarget 2016; 7: 5598-5612.
[48] Zuo J, Wang B, Long M, Gao Z, Zhang Z, Wang H, Wang X, Li R, Dong K and Zhang H. The type 1 transmembrane glycoprotein B7-H3 interacts with the glycolytic enzyme ENO1 to promote malignancy and glycolysis in HeLa cells. FEBS Lett 2018; 592: 2476-2488.
[49] Karijolich J, Kantartzis A and Yu YT. RNA modifications: a mechanism that modulates gene expression. Methods Mol Biol 2010; 629: 1-19.
[50] Bohnsack KE, Hobartner C and Bohnsack MT. Eukaryotic 5-methylcytosine (m(5)C) RNA methyltransferases: mechanisms, cellular functions, and links to disease. Genes (Basel) 2019; 10: 102.
[51] Squires JE, Patel HR, Nousch M, Sibbritt T, Humphreys DT, Parker BJ, Suter CM and Preiss T. Widespread occurrence of 5-methylcytosine in human coding and non-coding RNA. Nucleic Acids Res 2012; 40: 5023-5033.

[52] Delaunay S and Frye M. RNA modifications regulating cell fate in cancer. Nat Cell Biol 2019; 21: 552-559.
[53] Mei L, Shen C, Miao R, Wang JZ, Cao MD, Zhang YS, Shi LH, Zhao GH, Wang MH, Wu LS and Wei JF. RNA methyltransferase NSUN2 promotes gastric cancer cell proliferation by repressing p57(Kip2) by an m(5)C-dependent manner. Cell Death Dis 2020; 11: 270.
[54] Doll A and Grzeschik KH. Characterization of two novel genes, WBSCR20 and WBSCR22, deleted in Williams-Beuren syndrome. Cytogenet Cell Genet 2001; 95: 20-27.
[55] Muller M, Beck IM, Gadesmann J, Karschuk N, Paschen A, Proksch E, Djonov V, Reiss K and Sedlacek R. MMP19 is upregulated during melanoma progression and increases invasion of melanoma cells. Mod Pathol 2010; 23: 511-521.
[56] Nebenfuehr S, Kollmann K and Sexl V. The role of CDK6 in cancer. Int J Cancer 2020; 147: 2988-2995.
[57] Wu X, Yang X, Xiong Y, Li R, Ito T, Ahmed TA, Karoulia Z, Adamopoulos C, Wang H, Wang L, Xie L, Liu J, Ueberheide B, Aaronson SA, Chen X, Buchanan SG, Sellers WR, Jin J and Poulikakos PI. Distinct CDK6 complexes determine tumor cell response to CDK4/6 inhibitors and degraders. Nat Cancer 2021; 2: 429-443.
[58] Schmoellerl J, Barbosa IAM, Eder T, Brandstoetter T, Schmidt L, Maurer B, Troester S, Pham HTT, Sagarajit M, Ebner J, Manhart G, Aslan E, Terlecki-Zaniewicz S, Van der Veen C, Hoermann G, Duployez N, Petit A, Lapillonne H, Puissant A, Itzykson R, Moriggl R, Heuser M, Meisel R, Valent P, Sexl V, Zuber J and Grebien F. CDK6 is an essential direct target of NUP98 fusion proteins in acute myeloid leukemia. Blood 2020; 136: 387-400.
[59] Wang YL, Liu JY, Yang JE, Yu XM, Chen ZL, Chen YJ, Kuang M, Zhu Y and Zhuang SM. Lnc-UCID promotes G1/S transition and hepatoma growth by preventing DHX9-mediated CDK6 down-regulation. Hepatology 2019; 70: 259-275.
[60] Xu X, Shen X, Wang J, Feng W, Wang M, Miao X, Wu Q, Wu L, Wang X, Ma Y, Wu S, Bao X, Wang W, Wang Y and Huang Z. YAP prevents premature senescence of astrocytes and cognitive decline of Alzheimer's disease through regulating CDK6 signaling. Aging Cell 2021; 20: e13465.
[61] Jonasch E, Walker CL and Rathmell WK. Clear cell renal cell carcinoma ontogeny and mechanisms of lethality. Nat Rev Nephrol 2021; 17: 245-261.
[62] Krishna C, DiNatale RG, Kuo F, Srivastava RM, Vuong L, Chowell D, Gupta S, Vanderbilt C, Purohit TA, Liu M, Kansler E, Nixon BG, Chen YB, Makarov V, Blum KA, Attalla K, Weng S, Salmans ML, Golkaram M, Liu L, Zhang S, Vijayaraghavan R, Pawlowski T, Reuter V, Carlo MI, Voss MH, Coleman J, Russo P, Motzer RJ, Li MO, Leslie CS, Chan TA and Hakimi AA. Single-cell sequencing links multiregional immune landscapes and tissue-resident T cells in ccRCC to tumor topology and therapy efficacy. Cancer Cell 2021; 39: 662-677, e6.

Table S1. siRNA sequence in the study

Name	Sequcence 5' to 3'
ENO3-1#-F	GGGUGAACAUCCAGAUUGUUU
ENO3-1#-R	AAGGGUGAACAUCCAGAUUGU
ENO3-2#-F	GAGCUGUAUAAGAGCUUUAUU
ENO3-2#-R	AAGAGCUGUAUAAGAGCUUUA
NSUN2-F	CCGGCCACUUUAAGAAUUAUU
NSUN2-R	AACCGGCCACUUUAAGAAUUA
NSUN5-F	GCGGAACUGAGGUAAACUAUU
NSUN5-R	AAGCGGAACUGAGGUAAACUA
NSUN7-F	GCCCUGAAGAAGUUUAUAAUU
NSUN7-R	AAGCCCUGAAGAAGUUUAUAA
TET2-F	GGGCCUUACAACAGAUAUAUU
TET2-R	AAGGGCCUUACAACAGAUAUA

Table S2. Primers used in the study

Name	Sequcence 5' to 3'
PKM-F1	*Tctcttcgtctttgcagcgt*
PKM-R1	*Cagctgctgggtctgaatga*
ENO1-F	*Tgcacttgcaggtttatggc*
ENO1-R	Ccctgttctcatgcttgggt
ENO2-F	*Tactcattggggttccgcac*
ENO2-R	*Cacatcgttcccccaagtca*
ENO3-F	*Atcttggactccaggggcaa*
ENO3-R	*Ggccccaaacttggctttcc*
PGAM1-F	*Tgaagcaaaacgcaggacag*
PGAM1-R	*Catcataggagcgcctccag*
PGAM2-F	*Ggttcgatgcagagctgagt*
PGAM2-R	*Gtaccgacgctccttgctaa*
PGAM4-F	*Gaagcctatcaagcccatgc*
PGAM4-R	*Ggtcgtggcttagcatgttcc*
PGK1-F	*Ccactgtggcttctggcata*
PGK1-R	*Atgagagctttggttccccg*
PGK2-F	*Ggaaccaaagccctcatgga*
PGK2-R	*Caggcaaatgcgtgaccaaa*
NSUN5-F	*Cctcacaggccaaagcatca*
NSUN5-R	*Gggaaccctgagtgagtgtg*
LDHA-F	*Catggcctgtgccatcagta*
LDHA-R	*Agatatccactttgccagagaca*
LDHB-F	*Gtaggtttcggctcaggacc*
LDHB-R	*Cctcttcttccgcaactggt*
NSUN2-F	*Gctaccccgagatcgtcaag*
NSUN2-R	*Tcaggatacctttgtaaccagt*
NSUN3-F	*Tgccaaggctacactggtaag*
NSUN3-R	*Cccactgtgtggctaggaag*
NSUN4-F	*Ttcttctatgaccggcacgc*
NSUN4-R	*Ccagtcgaacagcagggaat*
NSUN7-F	*Ggacaaccttacagcgggac*
NSUN7-R	*Accattctgtcttctggccg*
TET2-F	*Gaaaggagacccgactgcaa*
TET2-R	*Atcttgagagggtgtgctgc*
DNMT1-F	*Tatccgaggagggctacctg*
DNMT1-R	*Atgagcaccgttctccaagg*
DNMT3B-F	*Tggagccacgacgtaacaaa*
DNMT3B-R	*Aggcatccgtcatctttcagc*
β-actin-F	*Aatgggcagccgttaggaaa*
β-actin-R	*Gcgcccaatacgaccaaatc*